ACS APPLIED MATERIALS & INTERFACES

Research Article

www.acsami.org

Lattice Strain Induced Remarkable Enhancement in Piezoelectric Performance of ZnO-Based Flexible Nanogenerators

Yang Zhang,[†] Caihong Liu,[†] Jingbin Liu,[§] Jie Xiong,[§] Jingyu Liu,[†] Ke Zhang,[†] Yudong Liu,[†] Mingzeng Peng,[†] Aifang Yu,[†] Aihua Zhang,[†] Yan Zhang,[†] Zhiwei Wang,[†] Junyi Zhai,*[,†] and Zhong Lin Wang*[,†,‡]

[†]Beijing Institute of Nanoenergy and Nanosystems, Chinese Academy of Sciences, Beijing 100083, China

[‡]School of Materials Science and Engineering, Georgia Institute of Technology, Atlanta, Georgia 30332-0245, United States

[§]State Key Laboratory of Electronic Thin Films and Integrated Device, University of Electronic Science and Technology of China, Chengdu 610054, China

S *Supporting Information*

ABSTRACT: In this work, by employing halogen elements (fluorine, chlorine, bromine, and iodine) as dopant we demonstrate a unique strategy to enhance the output performance of ZnO-based flexible piezoelectric nanogenerators. For a halogen-doped ZnO nanowire film, dopants and doping concentration dependent lattice strain along the ZnO *c*-axis are established and confirmed by the EDS, XRD, and HRTEM analysis. Although lattice strain induced charge separation was theoretically proposed, it has not been experimentally investigated for wurtzite structured ZnO nanomaterials. Tuning the lattice strain from compressive to tensile state along the ZnO *c*-axis can be achieved by a substitution of halogen dopant from fluorine to other halogen elements due to the ionic size difference between dopants and oxygen. With its focus on a group of nonmetal element induced lattice strain in ZnO-based nanomaterials, this work paves the way for enhancing the performance of wurtzite-type piezoelectric semiconductor nanomaterials via lattice strain strategy which can be employed to construct piezoelectric nanodevices with higher efficiency in a cost-effective manner.

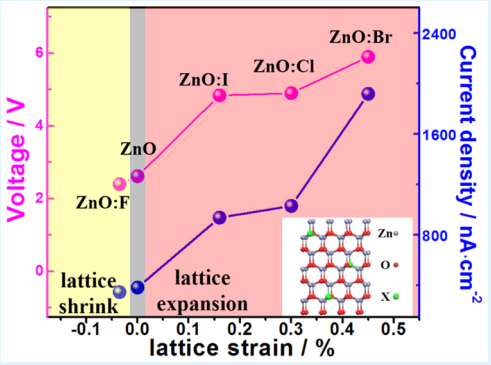

KEYWORDS: *piezoelectric nanogenerator, ZnO, lattice strain, piezocharges separation, chemical doping*

1. INTRODUCTION

Recent advances in material science enable us to harvest ambient mechanical energy from the environment, convert it into electric energy, and then power portable electronics.[1,2] Piezoelectric nanogenerators (PENGs) and triboelectric nanogenerators (TENGs) have attracted a great deal of attention from the scientific community and are considered as promising building blocks for the design and application of renewable, lightweight, and low-cost energy sources.[3−5] The output performance of the nanogenerator is highly dependent on nanomaterials employed in TENGs or PENGs.[5−9] With respect to large piezoelectric coefficients in PZT, PMN-PT, and PZN-PT materials, there is always a strong push to explore lead-free building materials because of environmental concerns.[10−15] Therefore, it is essential to develop high-performance PENGs and TENGs with environmental friendly materials, especially for the case of implantable or human skin wearable energy harvesting systems.[16−21]

ZnO is one of the most fascinating environmentally benign functional materials with distinguished performance in PENGs and piezotronic devices, such as piezoelectric field effect transistors, piezoelectric diodes, piezoelectric strain sensors, biological sensors, and photodetectors.[1,22−24] Therefore, the output performance of a ZnO-based piezoelectric nanodevice should be further optimized by modulating the characteristic of intrinsic ZnO.[25] In order to improve the utilization efficiency of piezoelectric charge, it is indispensable to synthesize non-centrosymmetric materials to broaden the investigation of the p- and n-type doped ZnO.[26] For instance, Sb-doped ZnO nanowire/belt exhibited its potential applications in thermoelectric nanogenerators, self-powered ultraviolet photodetectors, and gesture recognition devices.[27] Recent works revealed that the optical and electronic properties of semiconductor nanomaterials can be tuned via strain-engineering, e.g., buckled CdS nanowires, bent ZnO nanowires, and strain-driven redox behaviors in carbon nanomaterials.[28−33] It is known that piezocharges can be generated by externally applied tensile or compressive strain to the ZnO micro/nanowire or thin film, but less attention has been paid to the piezoelectric effect enhanced by lattice strain along the polar *c*-axis direction of wurtzite

Received: October 28, 2015
Accepted: December 24, 2015
Published: December 24, 2015

DOI: 10.1021/acsami.5b10345
ACS Appl. Mater. Interfaces 2016, 8, 1381−1387

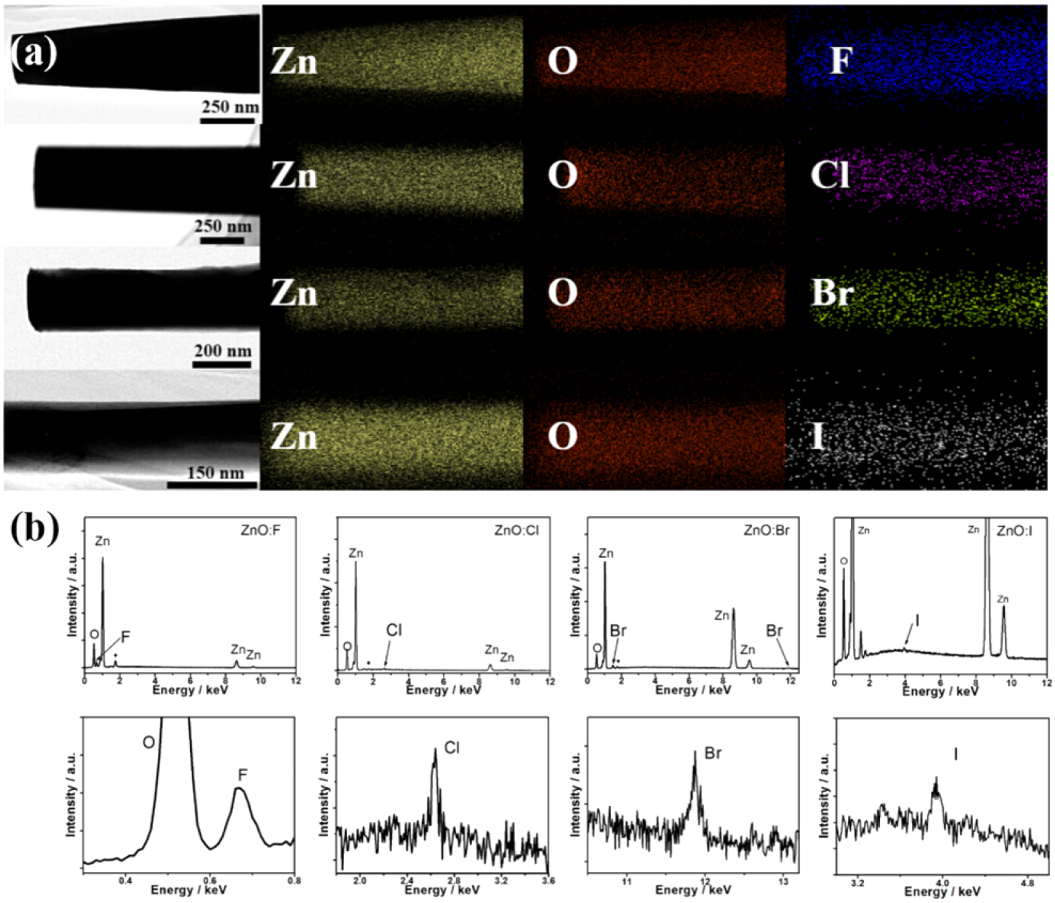

Figure 1. (a) TEM images of the ZnO:X nanowire, chemical mapping images of Zn, O, F, Cl, Br, and I. (b) EDX spectra of ZnO:X NW film (X = F, Cl, Br, and I).

ZnO.[34] It has become more compelling that chemical doping is one of the prevalent approaches in tailoring the optical, electrical, and magnetic properties achieved by diverse dopants and different doping concentration. Such advantages make chemical doping a promising route toward boosting the performance of ZnO-based piezoelectric nanogenerators and piezo-phototronic nanodevices. Considering the notable difference in ionic radii between oxygen and halogen ions (F^-, Cl^-, Br^-, and I^-), it would be expected that the compressive or tensile lattice strain can be achieved in a doped ZnO film that has an inevitable impact on the fundamental properties of doped ZnO materials and performance of ZnO-based piezoelectric nanodevice.

In this work, we highlight the unique synthetic strategy which leads to the enhancement of the output performance of ZnO-based flexible piezoelectric nanogenerator through tailoring the lattice strain along the ZnO polar *c*-axis. In a comparison to the study of F- and Cl-doped ZnO, the investigations of Br- and I-doped ZnO materials are rather scarce.[35,36] More importantly, a systematical investigation on a group of halogen elements as nonmetal dopants has been difficult, which may open a new dimension in the field of ZnO-based piezoelectric nanomaterials. Focusing on the lattice strain induced by different halogen dopants, we characterized a series of halogen element doped ZnO nanowire films by energy dispersive X-ray (EDX) spectroscopy, X-ray diffraction (XRD), X-ray photoelectron spectroscopy (XPS), photoluminescence spectroscopy (PL), and high-resolution transmission electron microscopy (HRTEM). The electron transport property of the halogen-doped ZnO nanowire film was investigated as well. Our experimental observation highlights the essential role of varied halogen dopants as the key element in inducing the lattice strain along the ZnO *c*-axis. The current synthetic strategy is in stark contrast to the previous reports with attention concentrated on metal-doped ZnO as the building block in PENG, but the role of dopant with different ionic size remains unexplored.[37,38]

2. EXPERIMENTAL SECTION

2.1. Material Synthesis and Characterization. The synthesis process of undoped and halogen-doped nanowire films is carried out by a modified hydrothermal method. First, a ZnO seed layer was deposited by standard RF magnetron sputter deposition using a high-purity ZnO target (99.99%) and Ar/O_2 (flow rate was fixed at 8:1) as the sputtering gases at ambient temperature. Second, the PET with ZnO seed layer was placed in the nutrient solution consisting of zinc nitrate hexahydrate (100 mM) and hexamethylenetetramine (100 mM) and 10 mM NaX (X = F, Cl, Br, and I). After 7 h reaction in an oven (at 95 °C), the as-prepared ZnO nanowire films were carefully rinsed by deionized water to remove the unreacted chemical on the surface of the sample. Prior to the assembly of flexible PENG, the undoped and halogen-doped ZnO nanowire films were placed in 40 °C conditions overnight. The morphology of the halogen-doped ZnO nanowire was examined by TEM (F20). The crystal structure of the undoped and halogen-doped ZnO nanowire film was obtained by XRD using a Bede D1 ZM-SJ-001 diffractometer. The XPS characterization was conducted by Thermo Scientific ESCALAB 250Xi.

2.2. Device Fabrication and Characterization of PENG. The fabrication of PENG was fulfilled by sputtering 100 nm Cu (99.99%

DOI: 10.1021/acsami.5b10345
ACS Appl. Mater. Interfaces 2016, 8, 1381−1387

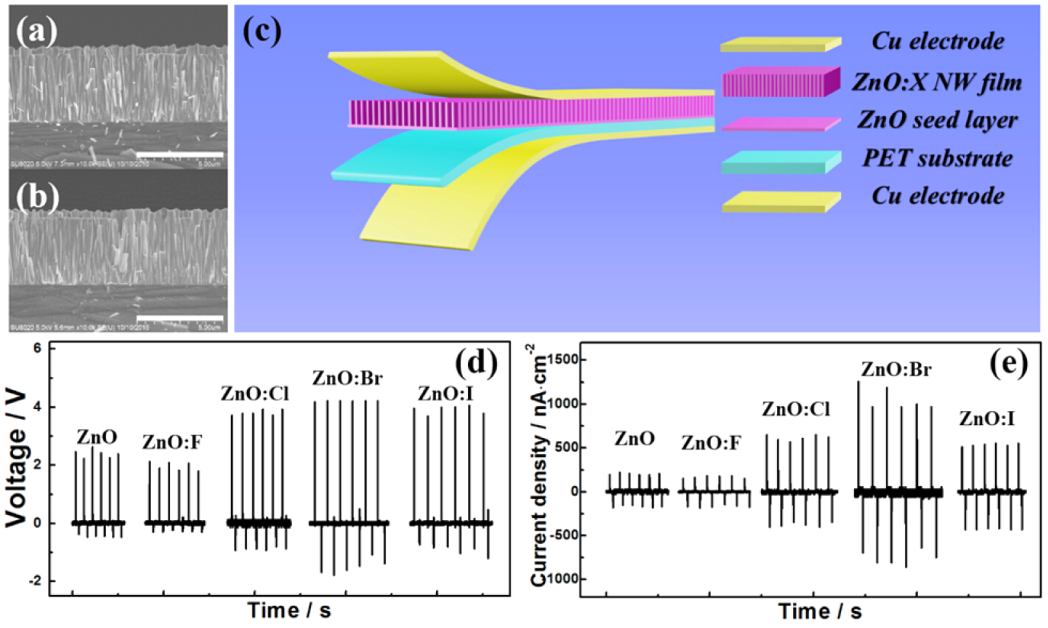

Figure 2. SEM cross-sectional view of (a) undoped ZnO and (b) ZnO:Br NW film. The scale bar is 5 μm. (c) Schematic diagram of the structure of halogen-doped ZnO NW film PENG. (d) Output voltage and (e) current of undoped ZnO and halogen-doped ZnO NW film as flexible piezoelectric nanogenerators.

purity) on the top of ZnO nanowire film and on the bottom of PET. In order to protect the Cu electrode and PENG during measurement, the PDMS layers were deposited on the top and bottom sides of the flexible PENG. The photograph of a ZnO-based PENG was presented in Figure S1 (see Supporting Information). The output voltage and current of the PENG were characterized by a LeCroy 610Zi oscilloscope, Stanford Research System SR 570, low-noise current amplifier. The room temperature electrical property was measured by a semiconductor characterization system (Keithley 4200-SCS).

3. RESULTS AND DISCUSSION

All of the halogen-doped ZnO nanowire (NW) films were synthesized by the modified hydrothermal routine in the presence of NaX (X = F, Cl, Br, and I). A detailed discussion of synthesis and fabrication of doped ZnO NW film PENG is described in the Experimental Section. Hereafter, the synthesized materials will be abbreviated as ZnO:X, where X denotes the corresponding halogen element (e.g., ZnO:Br is denoted as Br-doped ZnO). All as-synthesized doped ZnO compounds were synthesized using the hydrothermal method in the present of NaX containing nutrient solution. Figure 1 shows transmission electron microscopy (TEM) images of halogen-doped ZnO nanowires that were peeled off from the ZnO:X NW films. The chemical mapping images pointed out the distribution of halogen dopant throughout the whole ZnO nanowire in each sample, Figure 1a. The TEM characterization indicates the ZnO:X nanowire served as the building block in the textured films. The surface features of the as-synthesized ZnO:X NW film are similar to the undoped ZnO NW film. The EDX and XPS spectra of halogen-doped ZnO NW film exhibited signals from halogen dopant in each sample which agree well with TEM characterization. The doping concentration in each sample is 0.10% in ZnO:F, 0.20% in ZnO:Cl, 0.15% in ZnO:Br, and 0.08% in ZnO:I, Figure 1b and Figure S2 (SI).[39] Due to the small atomic number of fluorine, EDX characterization only can give the qualitative result on the presentation of F dopant, which is influenced by the sample size, quality, and its low doping concentration.[40,41] Figure S3 (SI) shows the PL spectra of undoped ZnO and ZnO:X NW film excited by a He−Cd laser at 325 nm. For ZnO:X NW film, the observation of the strong emission peak in the ultraviolet and broad green emission peaks in the visible region was comparable to previous reports.[42] The considerable difference was shown in the visible part as the incorporation of halogen dopant due to its different concentration and ionic size. Recently, Wang and co-workers reported that a heavily doped ZnO single nanowire with chlorine ions exhibited metallic conductivity. Compared to that of the undoped ZnO film, the conductivity of ZnO:X slightly increases by selecting a different dopant source in nutrient solution, see Figure S4 (SI). The morphology of undoped ZnO and Br-doped ZnO NW film was characterized. The cross-sectional and top views of ZnO NW film are presented in Figure 2 and Figures S5 and S6, respectively. The above-mentioned results provide solid evidence that the halogen ions were doped into the ZnO lattice in the process of hydrothermal synthesis and the doping concentration of halogen ions is quite low in ZnO:X.

The output performance of PENG essentially depends on the sandwiched piezoelectric materials between two electrodes. The device structure is schematically presented in Figure 2c, as well as the comparison of their output performance. The PET layer is multifunctional in the design of PENG including serving as flexible platform and avoiding the electron leakage. With application of a stress (1 MPa) to the PENG surface, the positive and negative piezocharges are generated and accumulated at the ZnO:X/PET interface and ZnO:X/Cu interface, respectively. The obtained V_{pp} (peak-to-peak voltage) and I_{pp} (peak-to-peak current) values for as-grown ZnO are estimated at 2.40 V and 400 nA/cm^2, respectively. The piezoelectric output performance of ZnO:X NW film is demonstrated in comparison to that of undoped ZnO NW film as well. When NaBr was added into the nutrient solution, the performance of the ZnO:Br NW film can be achieved in the aspects of both output voltage (up to 5.90 V) and current (up to 1910 nA/cm^2). The measurements of the output of ZnO

DOI: 10.1021/acsami.5b10345
ACS Appl. Mater. Interfaces 2016, 8, 1381−1387

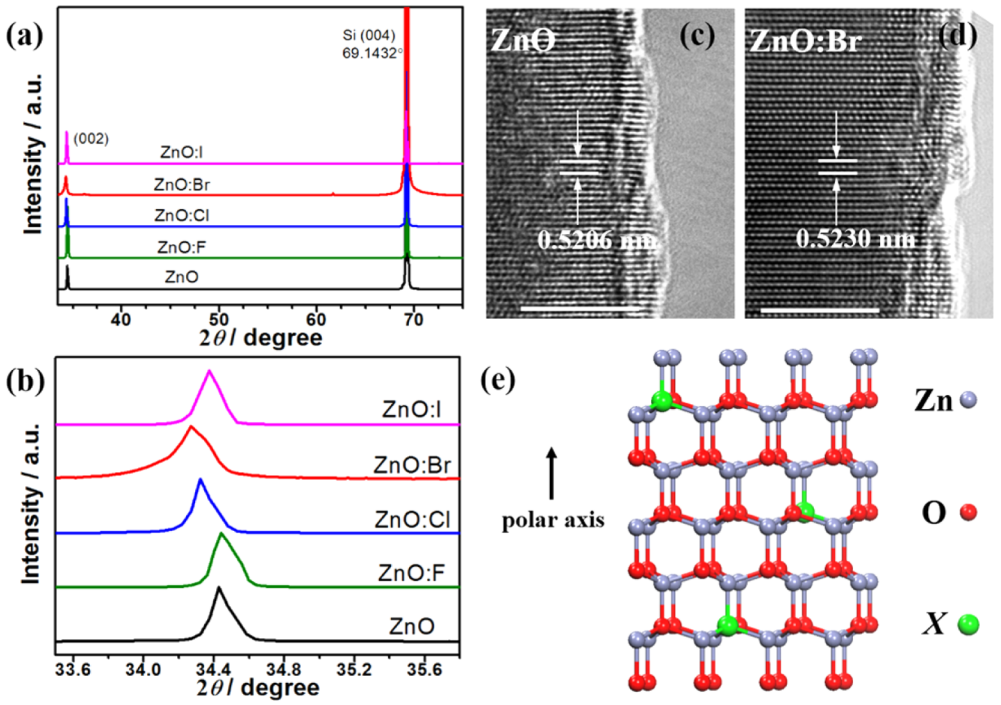

Figure 3. (a, b) XRD spectra of ZnO and halogen-doped ZnO NW film; (c, d) HRTEM images of the individual undoped ZnO and ZnO:Br nanowire which peeled from NW film, the scale bar is 5 nm; (e) crystal structure of ZnO:X (X = F, Cl, Br, and I).

NW film PENG with and without halogen element dopants were conducted under repeatedly applying a stress more than 30 cycles, see Figure S7 (SI). When the same amount of NaF was employed as the doping source, the output performance of ZnO:F NW film is lower than that of undoped ZnO NW film and other ZnO:X (X = Cl, Br, and I) NW films, see Figure 2d,e. The influence of different concentrations of the same halogen dopant on the piezoelectric performance improvement was carried out as well. The chlorine was chosen as the dopant to prepare ZnO:Cl NW films. With an increase in the NaCl concentration in nutrient solution, the enhancement in the output voltage of ZnO:Cl NW film was obtained, see Figure S8. According to the previous reports, the morphology, density, and size of ZnO NW will have impact on the output performance of PENG.[43] The length of the ZnO NW or the thickness of the ZnO NW film will influence the output voltage, while the diameters of ZnO NW will influence the output current. On the basis of our results, all of as-prepared undoped ZnO and halogen-doped ZnO films are composed of closely compacted ZnO nanowires with identical thickness and diameters mainly ranging from 150 to 350 nm, see Figure 2a,b. The output performance of undoped and doped ZnO NW textured film depends on the film thickness, which is different from the case of ZnO NW arrays film. Because we synthesized a halogen-doped ZnO NW film with identical thickness and fully covered on the PET substrate (see Figure S6), it can be considered that the difference in their piezoelectric performance resulted from the corresponding dopant.

The crystal structure of ZnO NW film was analyzed by X-ray diffraction using Cu Kα radiation (λ = 1.5406 Å). In order to accurately evaluate the influence of halogen dopant on the crystal nature of ZnO NW film, the diffraction peaks had been calibrated by the peak position of Si (004) for the as-prepared samples, see Figure 3. The lattice spacings of ZnO (0002) calculated from the diffraction patterns are 5.2058 Å in undoped sample while 5.2040 Å in ZnO:F, 5.2214 Å in ZnO:Cl, 5.2291 Å ZnO:Br, and 5.2139 Å in ZnO:I. Figure 3c,d shows HRTEM images of the individual undoped and ZnO:Br nanowire which were peeled from a NW film. In a comparison to the undoped ZnO sample, the slight change of c parameters can be attributed to the incorporation of halogen ions in ZnO NW film in the process of the hydrothermal synthesis. In fact, it would be expected that the corresponding ZnO (0002) plane spacing will be tuned due to the difference in ionic radius between oxygen ions ($r(O^{2-})$ = 0.140 nm) and halogen ions ($r(F^-)$ = 0.133 nm, $r(Cl^-)$ = 0.181 nm, $r(Br^-)$ = 0.193 nm, and $r(I^-)$ = 0.220 nm)) when the oxygen ions are replaced by halogen ions. We notice the lattice strain along ZnO polar c-axis has two contributions which can be interpreted by simultaneous analysis of the ionic size of dopant and doing concentration.

In comparison to vapor deposition techniques, hydrothermal synthesis has its advantage in the preparation of doped ZnO nanomaterials in low temperature.[35,44] As revealed from recent work, the doping concentration of chlorine ions can be controlled around 0.20% regardless of catalytic effect from other cations or anions. In nutrient solution, halogen ions X^- act as the dopant source, diffuse and bind to the surface of ZnO NW film, and then form $Zn(OH)_xX_y^{(x+y-2)}$ from $Zn(OH)_{2+x}^{x-}$ species temporarily. After the deposition of $Zn(OH)_{2+x}^{x-}$/$Zn(OH)_xX_y^{(x+y-2)-}$ and dehydration of the OH^- group, halogen ions were permanently preserved in the ZnO lattice, see Figure 3e. We suspect their different doping concentration resulted from the ionic radii of the varied halogen dopants that influence the amount of intermediate $Zn(OH)_xX_y^{(x+y-2)-}$ forming in the synthetic process.

$$\frac{1}{d_{(hkl)}^2} = \frac{4}{3}\left(\frac{l^2 + hk + k^2}{a^2}\right) + \frac{l^2}{c^2} \quad (1)$$

DOI: 10.1021/acsami.5b10345
ACS Appl. Mater. Interfaces 2016, 8, 1381−1387

$$c = \frac{\lambda}{\sin\theta} \quad (2)$$

$$c_{zz} = \frac{c - c_0}{c_0} \times 100\% \quad (3)$$

Under our conditions, the strain along the *c*-axis, c_{zz}, is given by eqs 1−3, where *c* is the lattice parameter of ZnO:X NW films calculated from X-ray diffraction data and c_0 is the lattice parameter of undoped ZnO synthesized by the same method without dopant source. The value of c_{zz} is used as a sensitive parameter to understand the variation of the strain state in the ZnO lattice.[45] In this way, the calculated strain in halogen-doped ZnO is about −0.035% in ZnO:F, 0.30% in ZnO:Cl, 0.45% in ZnO:Br, and 0.16% in ZnO:I. Even for iodine, with larger ionic radius than chlorine and bromine, the low doping concentration results in the relatively smaller lattice strain in ZnO:I NW film in comparison to ZnO:Cl and ZnO:Br samples, see Figure 4.

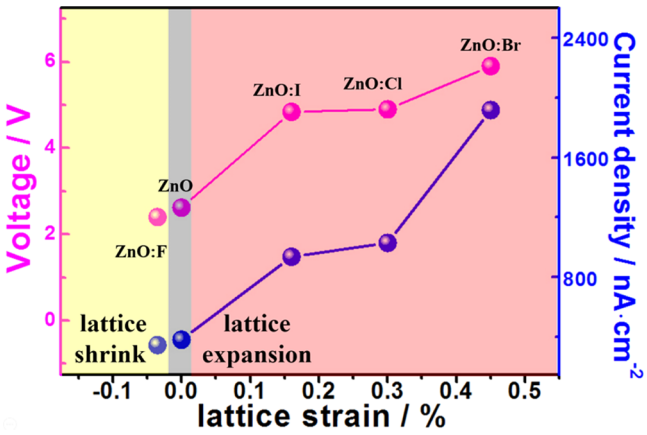

Figure 4. ZnO lattice strain dependence of the output performance of piezoelectric nanogenerator.

According to previous work on the individual ZnO nanowire, the local lattice spacing can be tuned by the elastic bending deformation, and the maximum strain was achieved about 1.0%.[34,46,47] The calculated lattice strain in ZnO:X samples is lower than that in the case of an externally bending ZnO nanowire which can be explained as the presentation of the limited amount of halogen ions along the *c*-axis of the ZnO nanowire. It is found that the compressive strain can be obtained by choosing F as the dopant since the ionic radius of F^- is slightly smaller than that of O^{2-}. These results are in good agreement with the ionic radius difference because the ionic radius of O^{2-} is larger than that of F^-, but smaller than those of Cl^-, Br^-, and I^-. With the undoped ZnO sample taken into account, the lattice strain in the ZnO:X varies from compression to tension state which was modulated by substituting the selected dopant from F to Cl, Br, and I ions with apparently increasing their ionic radii. Halogen ions play an indispensable role in modulating lattice strain along the ZnO polar *c*-axis. Previous works described the scenario of utilizing strain for charge separation in semiconductor materials at the nanoscale.[48−50] The ZnO:X nanomaterials synthesized in our condition have demonstrated that both ionic size and doping concentration were found as the driving force for increasing and decreasing the lattice strain along ZnO polar axis. Therefore, it can be concluded that the maximum lattice strain depends on the selected dopant as well as its doping concentration. With ionic radius larger than oxygen's, the existence of halogen element in ZnO lattice leads to the tensile strain that naturally causes a static polarization to the ZnO lattice and thus the piezocharges at the two ends. However, it should be mentioned that the dopant can induce the lattice distortion and the lattice disorder as well, which may have a negative contribution on the performance of ZnO-based PENG.[43,51] Precise estimation of the lattice strain and disorder contribution to ZnO:X film requires an in situ study on ZnO:X nanowires, which is underway, and complete analysis of these factors will be presented in the future. According to previous studies, the piezoelectric potential screening by free electrons in undoped ZnO has limited the energy conversion efficiency of the ZnO-based PENGs.[52−55] The deposition of CuO or other p-type materials can consume the free electrons in ZnO layer and further improve the output performance of PENG. Due to the CuO/ZnO pn heterojunction, a depletion region is formed near the junction boundary. Therefore, the built-in electric field near the heterojunction/interface effectively depletes free electrons in the ZnO layer, which reduces the screening effects for the generated piezoelectric potential and leads to an enhancement of piezoelectric output voltage. In order to illustrate whether chemical doping increases the electron screening effect, we synthesized undoped ZnO, ZnO:Cl, and ZnO:Br nanowire films on a predeposited CuO layer. The enhanced output performances were obtained for ZnO nanowires film with and without halogen dopants. For undoped ZnO NW film, the output voltage increased from 2.4 to 4.8 V. For ZnO:Cl and ZnO:Br NW film, their output voltages increased from 4.9 to 7.2 V and from 5.9 to 8.1 V, respectively. The enhancement of halogen-doped ZnO NW film is comparable to the undoped ZnO NW film, which indicates the chemical doping does not cause a significant electron screening effect and the improvement in their piezoelectric originated from the corresponding dopants. The larger XRD shift and lattice strain can be achieved by increasing the ionic size of dopants and doping concentration. However, if the ionic size of the dopant is too large and/or the doping concentration is too high, the existence of dopants may result in more lattice defects, which increases the concentration of free electrons and the screening effect and decreases the output performance. In our case, the halogen element doped ZnO NW film can have larger lattice strain and without extra electron screening effect. Therefore, dopants (Cl, Br, and I) played an essential role in enhancing the piezoelectric output of ZnO NW film. For instance, previous work demonstrated that the S-doped ZnO NW demonstrated a large XRD shift and high doping concentration, which exhibited slight enhancement in piezoelectric output compared to that of the undoped ZnO NW.[43] This indicates chemical doping can be regarded as a practical routine for enhancing piezoelectric performance only by controlling the ionic size of dopants and controlling the doping concentration. The dopant induced the lattice strain, and the electron screening effect has a different contribution to the mechanically generated piezopotential, which is a competitive process. For the enhancement of the performance of piezoelectric nanogenerator and nanodevice, introducing p-type nanomaterials onto the ZnO film has been reported recently.[47−49] However, our synthetic strategy achieved the objective of enhancing the piezoelectric performance of ZnO film in a one-step solution process at low cost.[54−56]

DOI: 10.1021/acsami.5b10345
ACS Appl. Mater. Interfaces 2016, 8, 1381−1387

4. CONCLUSIONS

We have performed a unique synthetic strategy that modulates the lattice strain along ZnO polar *c*-axis by a low-cost chemical doping approach. Tuning the lattice strain from a compressive to tensile state can be achieved by the variation of halogen dopant from fluorine to other halogen elements by taking advantage of the ionic size between the dopant and oxygen element. For halogen-doped ZnO nanowire film, dopants and doping concentration-related lattice strain along ZnO *c*-axis are established and confirmed by the experimental characterization. As the successful and comprehensive investigation on a group of nonmetal element induced lattice strain in ZnO-based functional materials, this work paves the way for enhancing the performance of wurtzite-type piezoelectric semiconductor nanomaterials via lattice strain which can be potentially employed to construct piezoelectric nanodevices with higher efficiency in a cost-effective manner.

■ ASSOCIATED CONTENT

Supporting Information

The Supporting Information is available free of charge on the ACS Publications website at DOI: 10.1021/acsami.5b10345.

XPS, PL spectra, *I*−*V* curves, output performance of PENGs, and SEM images of doped ZnO NW films (PDF)

■ AUTHOR INFORMATION

Corresponding Authors

*E-mail: jyzhai@binn.cas.cn.
*E-mail: zlwang@gatech.edu.

Author Contributions

Yang Zhang and Caihong Liu contributed equally.

Notes

The authors declare no competing financial interest.

■ ACKNOWLEDGMENTS

This work was supported by NSFC (51472056, 51402064), the "Thousands Talents" program for pioneer researcher and his innovation team, China, and the Recruitment Program of Global Youth Experts, China.

■ REFERENCES

(1) Wang, Z. L. Nanopiezotronics. *Adv. Mater.* **2007**, *19*, 889−892.
(2) Wang, Z. L. Progress in Piezotronics and Piezo-phototronics. *Adv. Mater.* **2012**, *24*, 4632−4646.
(3) Wang, X. D. Piezoelectric Nanogenerators-Harvesting Ambient Mechanical Energy at the Nanometer Scale. *Nano Energy* **2012**, *1*, 13−24.
(4) Fan, F. R.; Tian, Z. Q.; Wang, Z. L. Flexible Triboelectric Generator! *Nano Energy* **2012**, *1*, 328−334.
(5) Wang, Z. L. Triboelectric Nanogenerators as New Energy Technology for Self-Powered Systems and as Active Mechanical and Chemical Sensors. *ACS Nano* **2013**, *7*, 9533−9557.
(6) Wu, J. M.; Chen, C. Y.; Zhang, Y.; Chen, K. H.; Yang, Y.; Hu, Y. F.; He, J. H.; Wang, Z. L. Ultrahigh Sensitive Piezotronic Strain Sensors Based on a $ZnSnO_3$ Nanowire/Microwire. *ACS Nano* **2012**, *6*, 4369−4374.
(7) Lee, K. Y.; Kim, D.; Lee, J. H.; Kim, T. Y.; Gupta, M. K.; Kim, S. W. Unidirectional High-Power Generation via Stress-Induced Dipole Alignment from $ZnSnO_3$ Nanocubes/Polymer Hybrid Piezoelectric Nanogenerator. *Adv. Funct. Mater.* **2014**, *24*, 37−43.
(8) Xing, L. L.; Nie, Y. X.; Xue, X. Y.; Zhang, Y. PVDF Mesoporous Nanostructures as the Piezo-Separator for a Self-Charging Power Cell. *Nano Energy* **2014**, *10*, 44−52.
(9) Yu, A.; Song, M.; Zhang, Y.; Zhang, Y.; Chen, L.; Zhai, J.; Wang, Z. L. Self-Powered Acoustic Source Locator in Underwater Environment Based on Organic Film Triboelectric Nanogenerator. *Nano Res.* **2015**, *8*, 765−773.
(10) Qi, Y.; Kim, J.; Nguyen, T. D.; Lisko, B.; Purohit, P. K.; McAlpine, M. C. Enhanced Piezoelectricity and Stretchability in Energy Harvesting Devices Fabricated from Buckled PZT Ribbons. *Nano Lett.* **2011**, *11*, 1331−1336.
(11) Wu, W. W.; Bai, S.; Yuan, M. M.; Qin, Y.; Wang, Z. L.; Jing, T. Lead Zirconate Titanate Nanowire Textile Nanogenerator for Wearable Energy-Harvesting and Self-Powered Devices. *ACS Nano* **2012**, *6*, 6231−6235.
(12) Park, K. I.; Son, J. H.; Hwang, G. T.; Jeong, C. K.; Ryu, J.; Koo, M.; Choi, I.; Lee, S. H.; Byun, M.; Wang, Z. L.; Lee, K. J. Highly-Efficient, Flexible Piezoelectric PZT Thin Film Nanogenerator on Plastic Substrates. *Adv. Mater.* **2014**, *26*, 2514−2520.
(13) Gu, L.; Cui, N.; Cheng, L.; Xu, Q.; Bai, S.; Yuan, M.; Wu, W.; Liu, J.; Zhao, Y.; Ma, F.; Qin, Y.; Wang, Z. L. Flexible Fiber Nanogenerator with 209 V Output Voltage Directly Powers a Light-Emitting Diode. *Nano Lett.* **2013**, *13*, 91−94.
(14) Xu, S.; Yeh, Y. W.; Poirier, G.; McAlpine, M. C.; Register, R. A.; Yao, N. Flexible Piezoelectric PMN-PT Nanowire-Based Nanocomposite and Device. *Nano Lett.* **2013**, *13*, 2393−2398.
(15) Chen, X.; Xu, S.; Yao, N.; Shi, Y. 1.6 V Nanogenerator for Mechanical Energy Harvesting Using PZT Nanofibers. *Nano Lett.* **2010**, *10*, 2133−2137.
(16) Yang, Y.; Zhang, H. L.; Chen, J.; Lee, S. M.; Hou, T. C.; Wang, Z. L. Simultaneously Harvesting Mechanical and Chemical Energies by a Hybrid Cell for Self-Powered Biosensors and Personal Electronics. *Energy Environ. Sci.* **2013**, *6*, 1744−1749.
(17) Yu, R. M.; Pan, C. F.; Chen, J.; Zhu, G.; Wang, Z. L. Enhanced Performance of a ZnO Nanowire-Based Self-Powered Glucose Sensor by Piezotronic Effect. *Adv. Funct. Mater.* **2013**, *23*, 5868−5874.
(18) Yang, P. K.; Lin, L.; Yi, F.; Li, X.; Pradel, K. C.; Zi, Y.; Wu, C. I.; He, J. H.; Zhang, Y.; Wang, Z. L. A Flexible, Stretchable and Shape-Adaptive Approach for Versatile Energy Conversion and Self-Powered Biomedical Monitoring. *Adv. Mater.* **2015**, *27*, 3817−3824.
(19) Zhong, J.; Zhang, Y.; Zhong, Q.; Hu, Q.; Hu, B.; Wang, Z. L.; Zhou, J. Fiber-Based Generator for Wearable Electronics and Mobile Medication. *ACS Nano* **2014**, *8*, 6273−6280.
(20) Pu, X.; Li, L.; Song, H.; Du, C.; Zhao, Z.; Jiang, C.; Cao, G.; Hu, W.; Wang, Z. L. A Self-Charging Power Unit by Integration of a Textile Triboelectric Nanogenerator and a Flexible Lithium-Ion Battery for Wearable Electronics. *Adv. Mater.* **2015**, *27*, 2472−2478.
(21) Wu, T.; Zhang, H. Piezoelectricity in Two-Dimensional Materials. *Angew. Chem., Int. Ed.* **2015**, *54*, 4432−4434.
(22) Zhou, J.; Gu, Y. D.; Fei, P.; Mai, W. J.; Gao, Y. F.; Yang, R. S.; Bao, G.; Wang, Z. L. Flexible Piezotronic Strain Sensor. *Nano Lett.* **2008**, *8*, 3035−3040.
(23) Wang, Z. L.; Song, J. Piezoelectric Nanogenerators Based on Zinc Oxide Nanowire Arrays. *Science* **2006**, *312*, 242−246.
(24) Zhang, Z.; Liao, Q. L.; Yu, Y. H.; Wang, X. D.; Zhang, Y. Enhanced Photoresponse of ZnO Nanorods-Based Self-Powered Photodetector by Piezotronic Interface Engineering. *Nano Energy* **2014**, *9*, 237−244.
(25) Wen, X.; Wu, W.; Ding, Y.; Wang, Z. L. Piezotronic Effect in Flexible Thin-Film Based Devices. *Adv. Mater.* **2013**, *25*, 3371−3379.
(26) Pradel, K. C.; Wu, W.; Zhou, Y.; Wen, X.; Ding, Y.; Wang, Z. L. Piezotronic Effect in Solution-Grown P-Type ZnO Nanowires and Films. *Nano Lett.* **2013**, *13*, 2647−2653.
(27) Pradel, K. C.; Wu, W.; Ding, Y.; Wang, Z. L. Solution-Derived ZnO Homojunction Nanowire Films on Wearable Substrates for Energy Conversion and Self-Powered Gesture Recognition. *Nano Lett.* **2014**, *14*, 6897−6905.

DOI: 10.1021/acsami.5b10345
ACS Appl. Mater. Interfaces 2016, 8, 1381−1387

(28) Sun, L.; Kim, D. H.; Oh, K. H.; Agarwal, R. Strain-Induced Large Exciton Energy Shifts in Buckled CdS Nanowires. *Nano Lett.* **2013**, *13*, 3836−3842.
(29) Wei, B.; Zheng, K.; Ji, Y.; Zhang, Y.; Zhang, Z.; Han, X. Size-Dependent Bandgap Modulation of ZnO Nanowires by Tensile Strain. *Nano Lett.* **2012**, *12*, 4595−4599.
(30) Ieong, M.; Doris, B.; Kedzierski, J.; Rim, K.; Yang, M. Silicon Device Scaling to the Sub-10-nm Regime. *Science* **2004**, *306*, 2057−2060.
(31) Zhang, Y.; Schiemenz, S.; Popov, A. A.; Dunsch, L. Strain-Driven Endohedral Redox Couple Ce^{IV}/Ce^{III} in Nitride Clusterfullerenes $CeM_2N@C_{80}$ (M = Sc, Y, Lu). *J. Phys. Chem. Lett.* **2013**, *4*, 2404−2409.
(32) Zhang, Y.; Popov, A. A.; Dunsch, L. Endohedral Metal or a Fullerene Cage Based Oxidation? Redox Duality of Nitride Clusterfullerenes $Ce_xM_{3-x}N@C_{78-88}$ (x = 1, 2; M = Sc and Y) Dictated by the Encaged Metals and the Carbon Cage Size. *Nanoscale* **2014**, *6*, 1038−1048.
(33) Zhang, Y.; Popov, A. A. Transition-Metal and Rare-Earth-Metal Redox Couples inside Carbon Cages: Fullerenes Acting as Innocent Ligands. *Organometallics* **2014**, *33*, 4537−4549.
(34) Han, X.; Kou, L.; Lang, X.; Xia, J.; Wang, N.; Qin, R.; Lu, J.; Xu, J.; Liao, Z.; Zhang, X.; Shan, X.; Song, X.; Gao, J.; Guo, W.; Yu, D. Electronic and Mechanical Coupling in Bent ZnO Nanowires. *Adv. Mater.* **2009**, *21*, 4937−4941.
(35) Wang, F.; Seo, J. H.; Li, Z.; Kvit, A. V.; Ma, Z.; Wang, X. Cl-doped ZnO Nanowires with Metallic Conductivity and Their Application for High-Performance Photoelectrochemical Electrodes. *ACS Appl. Mater. Interfaces* **2014**, *6*, 1288−1293.
(36) Zheng, Y. Z.; Tao, X.; Hou, Q. A.; Wang, D. T.; Zhou, W. L.; Chen, J. F. Iodine-Doped ZnO Nanocrystalline Aggregates for Improved Dye-Sensitized Solar Cells. *Chem. Mater.* **2011**, *23*, 3−5.
(37) Chang, Y. T.; Chen, J. Y.; Yang, T. P.; Huang, C. W.; Chiu, C. H.; Yeh, P. H.; Wu, W. W. Excellent Piezoelectric and Electrical Properties of Lithium-Doped ZnO Nanowires for Nanogenerator Applications. *Nano Energy* **2014**, *8*, 291−296.
(38) Shin, S. H.; Kim, Y. H.; Lee, M. H.; Jung, J. Y.; Seol, J. H.; Nah, J. Lithium-Doped Zinc Oxide Nanowires-Polymer Composite for High Performance Flexible Piezoelectric Nanogenerator. *ACS Nano* **2014**, *8*, 10844−10850.
(39) Abd-Ellah, M.; Moghimi, N.; Zhang, L.; Heinig, N. F.; Zhao, L. Y.; Thomas, J. P.; Leung, K. T. Effect of Electrolyte Conductivity on Controlled Electrochemical Synthesis of Zinc Oxide Nanotubes and Nanorods. *J. Phys. Chem. C* **2013**, *117*, 6794−6799.
(40) Yu, C. L.; Fan, Q. Z.; Xie, Y.; Chen, J. C.; Shu, Q.; Yu, J. C. Sonochemical Fabrication of Novel Square-Shaped F doped TiO_2 Nanocrystals with Enhanced Performance in Photocatalytic Degradation of Phenol. *J. Hazard. Mater.* **2012**, *237*, 38−45.
(41) Yu, C. L.; Zhou, W. Q.; Yang, K.; Rong, G. Hydrothermal Synthesis of Hemisphere-Like F-Doped Anatase TiO_2 with Visible Light Photocatalytic Activity. *J. Mater. Sci.* **2010**, *45*, 5756−5761.
(42) Wu, K. Y.; Sun, Z. Q.; Cui, J. B. Unique Approach Toward ZnO Growth with Tunable Properties: Influence of Methanol in an Electrochemical Process. *Cryst. Growth Des.* **2012**, *12*, 2864−2871.
(43) Hsu, C. L.; Su, I. L.; Hsueh, T. J. Sulfur-Doped-ZnO-Nanospire-Based Transparent Flexible Nanogenerator Self-Powered by Environmental Vibration. *RSC Adv.* **2015**, *5*, 34019−34026.
(44) Cui, J. B.; Soo, Y. C.; Chen, T. P.; Gibson, U. J. Low-Temperature Growth and Characterization of Cl-doped ZnO Nanowire Arrays. *J. Phys. Chem. C* **2008**, *112*, 4475−4479.
(45) Malek, M. F.; Mamat, M. H.; Musa, M. Z.; Khusaimi, Z.; Sahdan, M. Z.; Suriani, A. B.; Ishak, A.; Saurdi, I.; Rahman, S. A.; Rusop, M. Thermal Annealing-Induced Formation of ZnO Nanoparticles: Minimum Strain and Stress Ameliorate Preferred c-axis Orientation and Crystal-Growth Properties. *J. Alloys Compd.* **2014**, *610*, 575−588.
(46) Xu, S. G.; Guo, W. H.; Du, S. W.; Loy, M. M. T.; Wang, N. Piezotronic Effects on the Optical Properties of ZnO Nanowires. *Nano Lett.* **2012**, *12*, 5802−5807.
(47) Dietrich, C. P.; Lange, M.; Klupfel, F. J.; von Wenckstern, H.; Schmidt-Grund, R.; Grundmann, M. Strain Distribution in Bent ZnO Microwires. *Appl. Phys. Lett.* **2011**, *98*, 031105.
(48) Wu, Z.; Neaton, J. B.; Grossman, J. C. Charge Separation via Strain in Silicon Nanowires. *Nano Lett.* **2009**, *9*, 2418−2422.
(49) Kou, L. Z.; Zhang, Y.; Li, C.; Guo, W. L.; Chen, C. F. Local-Strain-Induced Charge Carrier Separation and Electronic Structure Modulation in Zigzag ZnO Nanotubes: Role of Built-In Polarization Electric Field. *J. Phys. Chem. C* **2011**, *115*, 2381−2385.
(50) Kou, L. Z.; Li, C.; Zhang, Z. Y.; Chen, C. F.; Guo, W. L. Charge Carrier Separation Induced by Intrinsic Surface Strain in Pristine ZnO Nanowires. *Appl. Phys. Lett.* **2010**, *97*, 053104.
(51) Kim, D.; Lee, K. Y.; Gupta, M. K.; Majumder, S.; Kim, S. W. Self-Compensated Insulating ZnO-Based Piezoelectric Nanogenerators. *Adv. Funct. Mater.* **2014**, *24*, 6949−6955.
(52) Sohn, J. I.; Cha, S. N.; Song, B. G.; Lee, S.; Kim, S. M.; Ku, J.; Kim, H. J.; Park, Y. J.; Choi, B. L.; Wang, Z. L.; Kim, J. M.; Kim, K. Engineering of Efficiency Limiting Free Carriers and an Interfacial Energy Barrier for an Enhancing Piezoelectric Generation. *Energy Environ. Sci.* **2013**, *6*, 97−104.
(53) Lei, J. X.; Yin, B.; Qiu, Y.; Zhang, H. Q.; Chang, Y.; Luo, Y. M.; Zhao, Y.; Ji, J. Y.; Hu, L. Z. Flexible Piezoelectric Nanogenerator Based on Cu_2O-ZnO p-n Junction for Energy Harvesting. *RSC Adv.* **2015**, *5*, 59458−59462.
(54) Shin, S. H.; Lee, M. H.; Jung, J. Y.; Seol, J. H.; Nah, J. Piezoelectric Performance Enhancement of ZnO Flexible Nanogenerator by a CuO-ZnO p-n Junction Formation. *J. Mater. Chem. C* **2013**, *1*, 8103−8107.
(55) Lee, K. Y.; Kumar, B.; Seo, J. S.; Kim, K. H.; Sohn, J. I.; Cha, S. N.; Choi, D.; Wang, Z. L.; Kim, S. W. P-Type Polymer-Hybridized High-Performance Piezoelectric Nanogenerators. *Nano Lett.* **2012**, *12*, 1959−1964.
(56) Lin, P.; Chen, X.; Yan, X. Q.; Zhang, Z.; Yuan, H. G.; Li, P. F.; Zhao, Y. G.; Zhang, Y. Enhanced Photoresponse of Cu_2O/ZnO Heterojunction with Piezo-modulated Interface Engineering. *Nano Res.* **2014**, *7*, 860−868.

DOI: 10.1021/acsami.5b10345
ACS Appl. Mater. Interfaces 2016, 8, 1381−1387